European Polymer Journal 194 (2023) 112129

Contents lists available at ScienceDirect

European Polymer Journal

journal homepage: www.elsevier.com/locate/europolj

Chitosan/collagen/Mg, Se, Sr, Zn-substituted calcium phosphate scaffolds for bone tissue engineering applications: A growth factor free approach

Antonia Ressler [a,b,*], Roope Ohlsbom [c,d], Andreja Žužić [a], Arjen Gebraad [c,d], Erkka J. Frankberg [b], Toni-Karri Pakarinen [e], Hrvoje Ivanković [a], Susanna Miettinen [c,d], Marica Ivanković [a]

[a] Faculty of Chemical Engineering and Technology, University of Zagreb, HR-10000 Zagreb, Marulićev trg 19, Croatia
[b] Faculty of Engineering and Natural Sciences, Tampere University, Korkeakoulunkatu 6, P.O. Box 589, 33014 Tampere, Finland
[c] BioMediTech, Faculty of Medicine and Health Technology, Tampere University, Arvo Ylpön katu 34, 33520 Tampere, Finland
[d] Research, Development and Innovation Centre, Tampere University Hospital, Elämänaukio, Kuntokatu 2, 33520 Tampere, Finland
[e] Department of Musculoskeletal Diseases, Tampere University Hospital, Elämänaukio, Kuntokatu 2, 33520 Tampere, Finland

ARTICLE INFO

Keywords:
Bone
Chitosan
Collagen
Ionic substitution
Lysozyme
Osteogenic differentiation
Scaffold
Regeneration

ABSTRACT

According to the biomimetic bone scaffold design paradigm, a scaffold resembling natural bone tissue with molecular, structural and biological compatibility is needed to allow effective regeneration of bone tissue. Continuing our previous studies regarding scaffolds with chitosan matrix containing Mg, Se, Sr, Zn-substituted calcium phosphates (CaPs), the focus of this work was to further improve the properties of these growth factor-free scaffolds. By addition of collagen into the chitosan matrix at weight ratios of 100:0, 75:25, 50:50, 25:75 and 0:100, we aimed to better resemble natural bone tissue. Highly porous composite scaffolds based on chitosan and collagen, with 30 wt% of Mg, Se, Sr, Zn-substituted CaPs, were prepared by the freeze-gelation method. The scaffolds show a highly porous structure, with interconnected pores in the range of 20–350 μm and homogeneously dispersed CaPs. The added collagen further enhanced the stability measured during 28 days in simulated biological conditions. *Live/dead* and CyQUANT assays confirmed good viability and proliferation of human bone marrow-derived mesenchymal stem/stromal cells, while successful osteogenic differentiation was confirmed by alkaline phosphatase quantification and type I collagen immunocytochemical staining. Results indicated that the addition of collagen into the chitosan matrix containing Mg, Se, Sr, Zn-substituted CaPs improved the physicochemical and biological properties of the scaffolds.

1. Introduction

Incidence of bone fractures increases worldwide, leading to a significant economic burden [1-3]. Growth factors, especially bone morphogenetic proteins 2 and 7 approved by the U.S. Food and Drug Administration (FDA), are commonly used as bioactive molecules in bone grafts to increase the osteogenic response. However, the use of growth factors can result in ectopic bone formation and if not designed appropriately burst release can have negative side effects [4]. Commercial collagen-based grafts combined with growth factors have been withdrawn from clinical use due to reported complications [4,5]. The use of growth factors can be avoided by ion doping of materials that mimic both the organic and inorganic phases of native bone tissue [6].

Type I collagen is the main organic component of bone extracellular matrix (ECM), playing essential roles in bone metabolism and ensuring sufficient elasticity, strength and toughness [7,8]. Type I collagen and non-collagenous insoluble proteins, mainly produced by osteoblasts, are the building components of native bone tissue [9]. Five triple-helical collagen molecules are arranged to form the collagen microsized fibrils between which apatite nanocrystals can be found [8,10]. Type I collagen contains multiple biological cues that can directly interact with cells to regulate cell adhesion, proliferation and/or differentiation. Various types of naturally derived polymers (e.g. alginate, chitin, chitosan, cellulose, gelatin, silk, starch) have been used in scaffolds

* Corresponding author at: Faculty of Engineering and Natural Sciences, Tampere University, Korkeakoulunkatu 6, P.O. Box 589, 33014 Tampere, Finland.
E-mail addresses: antonia.ressler@tuni.fi, aressler@fkit.unizg.hr (A. Ressler), roope.ohlsbom@tuni.fi (R. Ohlsbom), azuzic@fkit.unizg.hr (A. Žužić), arjen.gebraad@tuni.fi (A. Gebraad), erkka.frankberg@tuni.fi (E.J. Frankberg), tkpakarinen@me.com (T.-K. Pakarinen), hivan@fkit.unizg.hr (H. Ivanković), susanna.miettinen@tuni.fi (S. Miettinen), mivank@fkit.unizg.hr (M. Ivanković).

https://doi.org/10.1016/j.eurpolymj.2023.112129
Received 28 April 2023; Accepted 3 May 2023
Available online 13 May 2023

designed for bone tissue engineering applications to mimic type I collagen [11]. One of the most widely studied biopolymers is chitosan. Chitosan, a carbohydrate biopolymer, consists of randomly distributed D-glucosamine and *N*-acetyl-D-glucosamine structure units linked by β-(1–4) glycoside bonds. Due to high nitrogen concentrations, chitin and chitosan are differentiated by having a basic nature, in contrast to the majority of naturally occurring polysaccharides, which have a neutral or acidic nature. Chitosan is structurally similar to glycosaminoglycans, which are key components of bone ECM and cell surface that modulate the bioavailability and activity of various osteoblastic and osteoclastic factors [12-17]. Fasolino et al. [18] prepared chitosan-based scaffolds to examine anti-inflammatory and osteoinductive properties for bone regeneration applications. The designed scaffolds, bioactivated with osteoinductive signals, were able to inhibit an inflammatory response *in vitro* by preventing the inflammation trigger in cells and reducing oxidative stress metabolites. Further, Erickson et al. [19] demonstrated different possibilities of chitosan based-scaffolds by designing a composite bilayer scaffold where each layer was optimized with biomechanical and bioactive cues to enhance the proliferation of intended cell types, chondrogenic or osteogenic cells.

Chitosan or type I collagen alone are not osteoinductive and require combination with a bioactive inorganic phase (e.g. CaPs, bioactive glass, calcium silicates) to modulate stem cell differentiation towards an osteoblast phenotype [20,21]. In our previous work [22], chitosan-based scaffolds with Mg, Se, Sr, Zn-substituted calcium phosphates (CaP) were prepared by the freeze gelation method. Osteoinductive properties were significantly enhanced by the introduction of trace elements as indicated by the increased formation of bone tissue and expression of osteogenic marker genes in cultures with bone marrow-derived mesenchymal stem/stromal cells (hBMSCs) [22]. The trace elements play an important role in bone formation. Magnesium is a key element in the early stage of bone formation, and it can positively affect bone metabolism, osteoblast/osteoclast activity, cell adhesion, proliferation and differentiation of stem cells towards an osteoblast phenotype [23-25], while selenium is known for its strong antioxidant properties and its deficiency can delay bone growth and affect bone metabolism [26]. In our previous studies, the CaP system substituted with 1 mol% of SeO_3^{2-} ions showed selective anticancer properties with a toxic effect towards human osteosarcoma cells, and a non-toxic effect towards healthy human embryonic kidney 293 cells [27]. Further, strontium is known to increase the expression of bone-related genes such as type I collagen, runt-related transcription factor 2 and osteocalcin [28], while zinc is crucial for the function of alkaline phosphatase (ALP) [6]. ALPs are glycosyl-phosphatidylinositol-anchored Zn^{2+}-metallated glycoproteins that are released during the maturation process of osteoblasts and are essential in the mineralization of the ECM that the osteoblasts produce [6].

In addition to inorganic trace elements, it is important to mimic the organic phase of native bone tissue for the best regenerative response. The biomimicry of microstructure, phase and chemical composition of natural bone tissue has a key role in developing scaffolds with a desired regenerative response. The aim of this work was to further improve the biomimicry and osteoinductivity of bone scaffolds composed of chitosan and Mg, Se, Sr, Zn-substituted CaP developed in our previous study [22], by combining chitosan and collagen as composite matrix at different weight ratios: 0:100, 25:75, 50:50, 75:25 and 100:0. Highly porous chitosan-collagen composite scaffolds were prepared by the freeze-gelation method with addition of 30 wt% of substituted CaP particles and characterized. An extensive analysis of scaffold's degradation behavior during 28 days and a biological characterization were performed. Hypothesis was that the addition of collagen can have a positive effect on scaffolds' osteogenic properties. However, an appropriate ratio of chitosan to collagen within scaffolds for the best osteogenic response needs to be determined for the scaffolds containing multi-substituted CaP. To the best of our knowledge, there are no prior data in the literature regarding the osteogenic properties of composite scaffolds based on the combination of collagen, chitosan and multi-substituted CaP.

Table 1
Labels and composition of prepared composite chitosan (CHT)/collagen (COLL)/substituted calcium phosphate (CaP) scaffolds.

	Polymer phase content in composite scaffolds		CaP phase content (wt%)
	CHT (wt %)	COLL (wt %)	
CHT/COLL_100/0	70.0	0.0	30 wt% of CaP substituted with 5 mol% of Sr^{2+}, Zn^{2+}, Mg^{2+} and SeO_3^{2-} ions
CHT/COLL_75/25	52.5	17.5	
CHT/COLL_50/50	35.0	35.0	
CHT/COLL_25/75	17.5	52.5	
CHT/COLL_0/100	0.0	70.0	

2. Materials and methods

2.1. Preparation of composite scaffolds

The mono-substituted CaPs with 5 mol% of Sr^{2+}, Mg^{2+}, Zn^{2+} and SeO_3^{2-} ions were prepared as previously reported in our studies [22,27,29,30], using cuttlefish bones (calcium oxide, CaO) as a precursor of Ca^{2+} ions. In brief, the CaPs were prepared by dissolving the CaO and strontium nitrate ($Sr(NO_3)_2$, Sigma-Aldrich, St. Louis, Missouri, USA), sodium selenite pentahydrate ($Na_2SeO_3{\cdot}5H_2O$, Sigma Aldrich, St. Louis, Missouri, USA), zinc nitrate hexahydrate ($Zn(NO_3)_2{\cdot}6H_2O$, Honeywell, New Jersey, USA) or magnesium chloride hexahydrate ($MgCl_2{\cdot}6H_2O$, KEMIG, Croatia) in demineralized water. Urea phosphate (UPH, $CO(NH_2)_2$–H_3PO_4, Sigma-Aldrich, St. Louis, Missouri, USA) was added into the solution to gain (Ca + Sr)/P and Ca/(P + Se) molar ratio 1.67, required for stoichiometric hydroxyapatite (HAp). Stirring was continued for 5 days at 50 °C followed by overnight aging at room temperature (T = 23.5 °C ± 0.5). Ammonium dihydrogen phosphate ($NH_4H_2PO_4$, Lachner, Czech Republic) was added into the solution to gain (Ca + Zn)/P and (Ca + Zn)/P molar ratio 1.67. Stirring was continued for 3 days at 60 °C followed by overnight aging at room temperature. After synthesis, powders were filtered and dried at 90 °C for 12 h.

The appropriate amount of chitosan (M_w = 310–375 kg/mol, deacetylation degree > 0.75, source: crab shells, Sigma-Aldrich, St. Louis, Missouri, USA) was dissolved in 0.60 wt% acetic acid solution (99.8 %, Sigma-Aldrich, St. Louis, Missouri, USA) to obtain 1.2 wt% chitosan solution at ambient temperature. Further, the appropriate amount of collagen ($M_w \approx$ 300 kg/mol, source: bovine achilles tendon, Sigma-Aldrich, St. Louis, Missouri, USA) was left in 1.00 wt% of acetic acid solution (99.8 %, Sigma-Aldrich, St. Louis, Missouri, USA) to swell overnight at ambient temperature to obtain 1.2 wt% collagen suspension after mixing in the blender for 10 min. Then, chitosan and collagen solutions/suspensions were mixed to obtain a weight ratio of 100:0, 75:25, 50:50, 25:75 and 0:100. After the homogenization of polymers solutions/suspensions for 24 h by stirring at 1000 rpm, the homogenized mixure of four mono-substituted CaPs (the mass fraction of each was 25%) was added to each chitosan/collagen mixture to obtain 30 wt% of CaPs in the matrix, based on the previous study [31]. After the homogenization for 10 min by stirring at 1700 rpm, 10 min in the ultrasonic bath and 5 min by Sonoplus ultrasonic homogeniser (Sonoplus HD 4200, Bandelin, Berlin, Germany), composite suspensions were cooled to 4 °C. 18 mL of cooled composite suspensions were set in an aluminium foil covered Petri dish (diameter = 7 mm) molds and frozen at –30 °C. Aluminium foil cover on the Petri dish was used to enable frozen suspension detachment from mold after freezing. After 8 h at –30 °C,

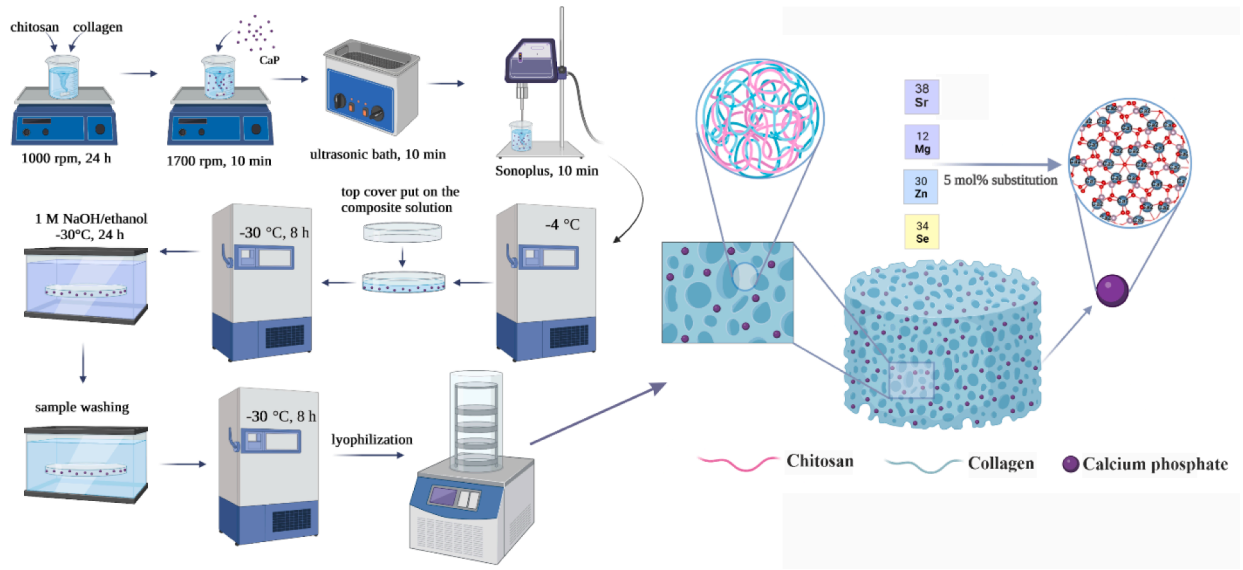

Fig. 1. Schematic illustration of preparation of composite chitosan/collagen/CaP scaffolds. Created with Biorender.com.

samples were immersed into the neutralisation medium of 1 M NaOH/ethanol at –30 °C for 24 h to induce the gelation of polymers. The samples were rinsed three times in 400 mL of ethanol 96 wt% (KEFO, Sisak, Croatia), three times in ethanol 70 wt%, washed five times with distilled water at ambient temperature, frozen (–30 °C), and lyophilized. The organic/inorganic content and labels of prepared composite scaffolds are shown in Table 1. The preparation of composite scaffolds is illustrated in Fig. 1.

2.2. Scaffold characterization

The Fourier transform infrared (FTIR) analysis of composite scaffolds was done using Bruker Vertex 70 spectrometer with attenuated total reflectance (ATR) unit. Scaffolds were pressed on a diamond and the absorbance data was collected at 20 °C in the range of 4000 – 400 cm^{-1}, with 32 scans and 4 cm^{-1} of spectral resolution.

Mineralogical phase analysis of composite scaffolds was performed *via* X-ray diffraction analysis (XRD) on a Shimadzu XRD-600 diffractometer with CuK_a (1.5406 Å) radiation. The diffractometer was operating at 40 kV and 30 mA and diffractograms were recorded in the 2θ range from 20° to 60° with a step size of 0.2° and exposure of 2 s. Obtained diffractograms were analyzed using the International Centre for Diffraction Data (ICDD) card catalogue for crystal phase characterization.

Scanning electron microscope (SEM) TESCAN Vega3 Easyprobe was used to investigate the morphology of composite scaffolds. The analysis was done at the electron beam energy of 10 keV and accelerating voltage of 10 kV. Before analysis, composite scaffolds were cut using a punch, fixed to a carbon stub and sputter–coated with gold and palladium for 120 s. Obtained SEM images were analyzed by ImageJ software (ImageJ2, Madison, Wis-consin, USA) to determine the diameter of 150 pores of obtained composite scaffolds. The pore size distribution results are shown as pore density (%) of each pore range ($n_{\text{pore range}}$) related to the total number of measured pores (n_{total}) according to Eq. (1).

$$pore\ \ desity(\%) = \frac{n_{pore\ \ range}}{n_{total}} \times 100 \quad (1)$$

2.3. In vitro enzymatic degradation

The degradation of prepared composite scaffolds was studied using two different lysozyme (Sigma-Aldrich, St. Louis, Missouri, USA) concentrations of 1.5 μg/mL and 150 μg/mL, corresponding to the activity of 164 U/mL and 16 400 U/mL, respectively. The analysis was conducted under static physiological conditions in phosphate buffer saline solution (PBS, Sigma-Aldrich, St. Louis, Missouri, USA). As the control sample, the composite scaffolds in the PBS solution without lysozyme were used. Composite scaffolds of 6 mm diameter and 2 mm thickness were incubated in 25 mL of PBS containing lysozyme at 37 °C for 28 days. To mimic physiological conditions *in vivo* and to maintain the activity of lysozyme, a freshly prepared degradation medium (lysozyme concentrations 0, 1.5 and 150 μg/mL) was changed every third day [32]. To determine the mass of swollen samples (m_s), the degradation medium was removed at defined time points (0, 14 and 28 days). After measuring m_s, scaffolds were immersed three times for 15 min in demineralized water at room temperature (T = 23.5 °C ± 0.5) in order to wash the degradation medium from the scaffolds. The scaffolds were then lyophilised (m_d) and Eg. (2) was used to determine the swelling ratio [22]:

$$Swelling\ \ ratio(\%) = \frac{m_s - m_d}{m_d} \times 100 \quad (2)$$

The scaffolds degradation was determined by dividing the remaining scaffold weight (m_d) and initial weight of the sample (m_{d0}) determined prior to enzymatic degradation as shown in Eq. (3) [22]:

$$Dry\ \ weight\ \ remaining\ \ ratio(\%) = \frac{m_d}{m_{d0}} \times 100 \quad (3)$$

To determine the influence of the degradation medium to the scaffolds, SEM and FTIR analyses of the scaffolds were conducted after the degradation, as well. SEM and FTIR analysis were performed as descried in 2.2. Scaffold characterization. Furthermore, scaffolds' degradation was monitored by differential scanning calorimetry (DSC). DSC was done using Netzsch thermoanalyzer 3500 Sirius in a temperature range from 20 °C to 350 °C. Measurements were done after 28 days of incubation at different lysozyme concentrations. Before analysis, scaffolds were uniformly cut to achieve a mass of ~ 1.5 mg and to fit in aluminium crucibles of 6 mm in diameter. The crucibles with samples were covered with aluminium lids and firmly sealed using the sealing press. All lids were pierced to prevent crucible deformation during the heating and sample decomposition. Prepared crucibles with samples were put into the instrument furnace next to the empty referent aluminium crucible and analyses were conducted in an N_2 atmosphere at a flow rate of 50 mL/min and a heating rate of 10 °C/min.

2.4. Biological characterization

2.4.1. Isolation and characterization of hBMSCs

The hBMSCs were isolated from a bone marrow aspirate sample obtained during a surgical procedure at the Department of Orthopedics and Traumatology, Tampere University Hospital. The bone marrow aspirate was obtained from a male donor (age 90) with written consent and under the approval of the Ethics Committee of the Pirkanmaa Hospital District, Tampere, Finland (R15174). Isolation of hBMSCs was done as previously described [33]. The isolated hBMSCs were preserved in vapor-phase nitrogen and thawed for characterization and experiments. The mesenchymal origin of the hBMSCs was verified by flow cytometric characterization of cell surface markers (Table S1 of Supplementary Data) and analyses of osteogenic and adipogenic differentiation potential (Figure S1 of Supplementary data). Both pre-analyses confirmed that the isolated hBMSCs are appropriate for determining the biological properties of the prepared scaffolds.

2.4.2. 3D culture of hBMSCs

Prior to cell seeding, scaffolds were sterilized in 70% ethanol for 24 h. After the sterilization, the scaffolds were washed three times with Dulbecco's phosphate-buffered saline (DPBS, Lonza, Basel, Switzerland) and left in osteogenic medium consisting of α-minimum essential medium (αMEM Gibco, Thermo Fisher Scientific, Waltham, Massachusetts, USA), 5% human serum (Serana, Brandenburg, Germany), 100 U/mL penicillin and 100 μg/mL streptomycin (Lonza, Basel, Switzerland), 200 μM ascorbic acid 2-phosphate (Sigma-Aldrich, St. Louis, Missouri, USA), 10 mM-glycerophosphate (Sigma-Aldrich, St. Louis, Missouri, USA) and 5 nM dexamethasone (Sigma Aldrich, St. Louis, Missouri, USA) for 24 h at 4 ℃. The following day, the scaffolds were warmed in the incubator (37 ℃) and moved to 96-well plates with a hydrophobic surface (Nunc, Thermo Fisher Scientific, Waltham, Massachusetts, USA). The scaffolds were seeded with 2.5×10^5 hBMSCs/scaffold at passage 4. Cells were added onto each scaffold in 10 μl of osteogenic medium and incubated (37 ℃, 5% CO_2) for 2 h to allow cell attachment and migration inside the scaffold. After the incubation, the osteogenic medium was added to a final volume of 200 μl per well and cell-seeded scaffolds were cultured for up to 21 days in standard cell culture conditions (37 ℃, 5% CO_2). The medium was changed every 3–4 days.

2.4.3. Qualitative analysis of cell viability

Qualitative analysis of cell viability (n = 2) was performed after 1 and 7 days of culture, by fluorescence detection using a Live/dead cell imaging kit (Invitrogen, Thermo Fisher Scientific, Waltham, Massachusetts, USA). The medium was removed from the wells, after which the scaffolds were washed with DPBS and incubated for 45 min at room temperature (RT) in a solution containing 0.5 μM Calcein-acetoxymethyl (CaAM) and 4×10^{-5} μM ethidium homodimer-1 (EthD-1). After the incubation, the scaffolds were imaged with Leica DMi8 fluorescent microscope equipped with a K5 sCmOS camera and LED5 light source (Leica, Wetzlar, Germany) using 480 nm and 555 nm excitation light for live cells stained with CaAM and dead cells stained with EthD-1, respectively.

Scaffolds without hBMSCs were used as negative controls (Figure S2 of Supplementary data). Live/dead analysis was similarly performed on the cell free scaffolds. In the negative controls, the signal of cell free scaffolds is shown to demonstrate the distinction between the fluorescence exhibited by scaffold structures and stained cells. Image processing was done with Fiji ImageJ software (version 2.3.0).

2.4.4. Proliferation assay

Quantitative analysis of cell number was performed on days 1 and 7 by analyzing the total amount of DNA in the samples using the CyQUANT Cell Proliferation Assay kit (Molecular Probes, Thermo Fisher Scientific, Waltham, Massachusetts, USA) as previously described [34,35]. Briefly, hBMSCs were lysed with Triton-X 100 (Sigma-Aldrich, St. Louis, Missouri, USA) and frozen (-70 ℃). After two freeze–thaw cycles, 20 μl of cell lysate was mixed with CyQUANT working solution in triplicates in a 96-well plate (Nunc, Thermo Fisher Scientific, Waltham, Massachusetts, USA). The resulting fluorescence was measured with Victor Nivo Multimode Microplate Reader (PerkinElmer, Waltham, Massachusetts, USA) at 480/520 nm.

2.4.5. Alkaline phosphatase activity

Alkaline phosphatase (ALP) activity was quantitatively determined on days 1 and 7, as previously described [34]. ALP activity was determined from the same Triton-X 100 cell lysates as the DNA amount. Briefly, 20 μl of cell lysate was mixed with a working solution in triplicates in a 96-well plate. The working solution comprised 1:1 stock substrate solution (p-nitrophenol phosphate, Sigma Aldrich, St. Louis, Missouri, USA) and 1.5 M alkaline buffer solution (2-amino-2-methyl propanol, Sigma Aldrich, St. Louis, Missouri, USA). ALP and p-nitrophenol phosphate produce a colorimetric reaction in the alkaline environment provided by the buffer solution [34]. The resulting absorbance was measured with Victor Nivo Multimode Microplate Reader at 405 nm to determine the amount of active ALP in the samples. Finally, ALP activity for each sample was normalized by the relative cell numbers measured earlier.

2.4.6. Immunocytochemical staining and confocal microscopy

Immunostaining was performed to evaluate type I collagen expression of the hBMSCs. Also, phalloidin staining of the actin cytoskeleton

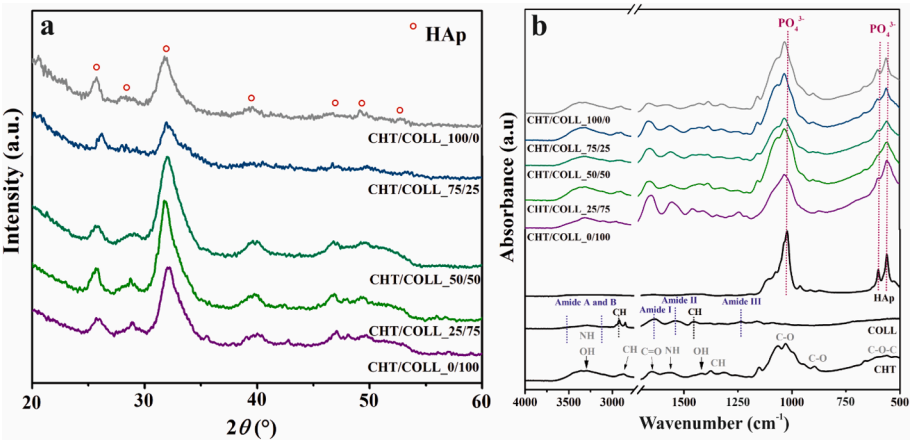

Fig. 2. XRD pattern (a) and FTIR spectra (b) of prepared composite scaffolds with different ratios of chitosan (CHT) and collagen (COLL) biopolymers. Pure CHT, COLL and HAp were used as a control for FTIR analysis. Characteristic HAp (ICDD 9-432) diffraction maxima are depicted in a) with red circles.

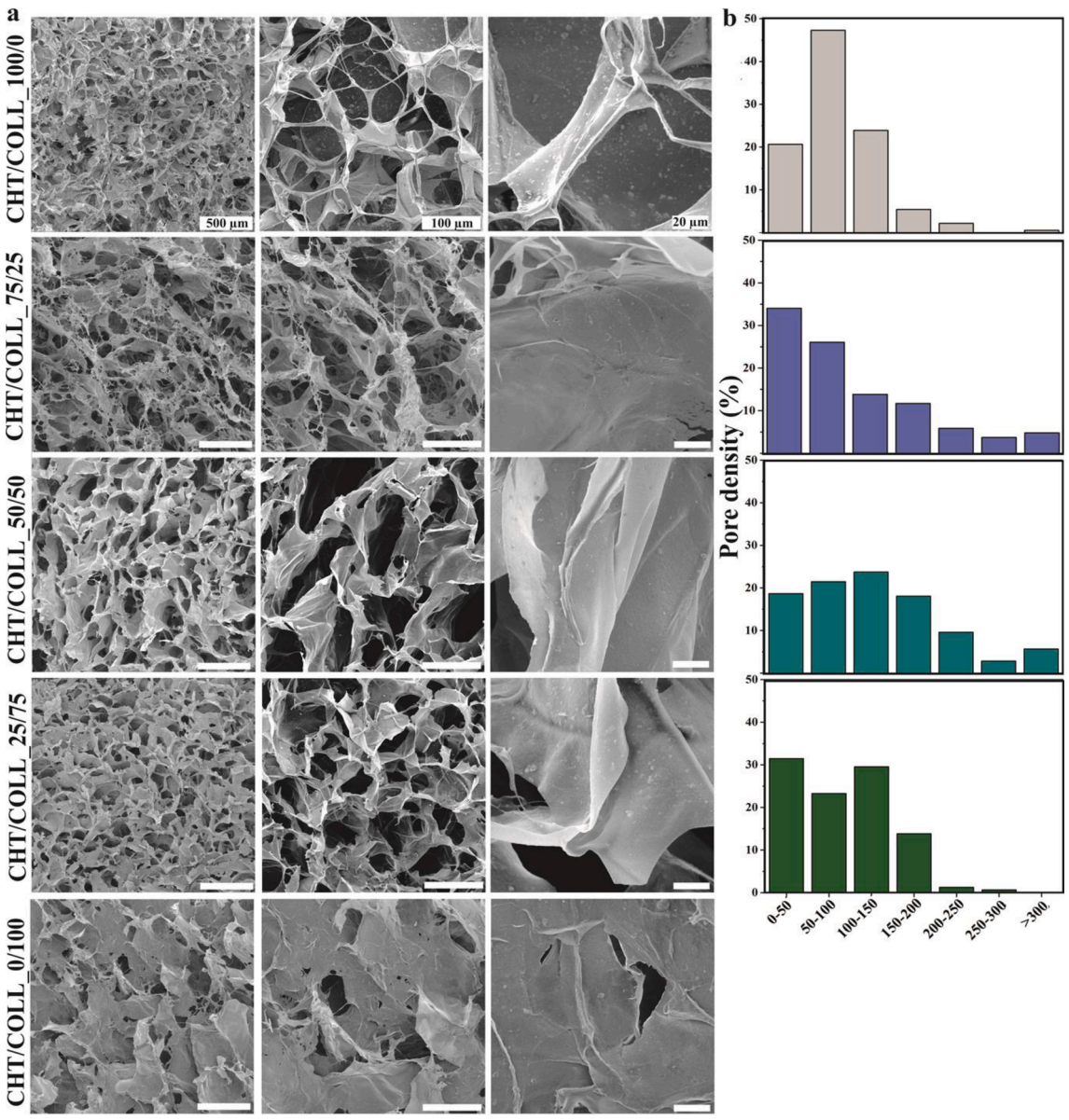

Fig. 3. Structure of chitosan/collagen scaffolds with addition of multisubstituted CaP particles. (a) Scanning electron microscope cross-sectional imaging of prepared composite scaffolds with a varying ratio between chitosan and collagen and (b) corresponding pore size distribution with pore density (%) as a function of pore diameter range (µm). Scale bars in (a): 500, 100 and 20 µm.

was performed to assess hBMSC morphology. The stainings were performed as previously described, with slight modifications [36]. First, the samples were fixed with 4% paraformaldehyde at RT for 20 min, after which the cells were permeabilized with 0.1 % Triton-X 100 at RT for 15 min. Samples were blocked with 2% bovine serum albumin (BSA) at RT for 1 h, after which the samples were incubated overnight in a rabbit monoclonal anti-collagen I antibody solution (1:250 in 1% BSA; Abcam, Cambridge, UK) at 4 ℃. The next day, the samples were incubated in a mixture of secondary antibody (donkey anti-rabbit Alexa Fluor 488 IgG; Invitrogen, Thermo Fisher Scientific, Waltham, Massachusetts, USA) and ATTO 643 phalloidin (ATTO-TEC GmbH, Siegen, Germany, 1:400 dilution of both in 1% BSA) at RT for 1 h. Finally, the cell nuclei were stained with 4′,6-diamidino-2-phenylindole (DAPI, 1:1500 in DPBS; Sigma-Aldrich, St. Louis, Missouri, USA) at RT for 30 min.

Samples were imaged using Zeiss LSM 780 Confocal Microscope (Zeiss Microscopy, Jena, Germany) with a 10x air immersion objective at a resolution of 2048 × 2048 pixels and image size of 1062.7 × 1062.7 µm (z-step size = 1.7 µm). The acquired images were deconvoluted using Hyugens Essential software (version 22.04, Scientific Volume Imaging, Hilversum, Netherlands) and further processed using Imaris Microscopy Image Analysis software (version 9.9.1, Oxford Instruments, Abingdon, UK). The Imaris software was also utilized for creating 3D animations of the images (Video S1 of Supplementary data).

2.5. Statistical analysis

All data were expressed as mean ± standard deviation. Statistical analysis was performed using a one-way ANOVA test followed by a post-hoc test to evaluate the statistical significance between groups. A value of $p < 0.05$ was considered statistically significant.

3. Results and discussion

3.1. The composition and morphology of composite scaffolds

The characterization of prepared composite scaffolds was performed

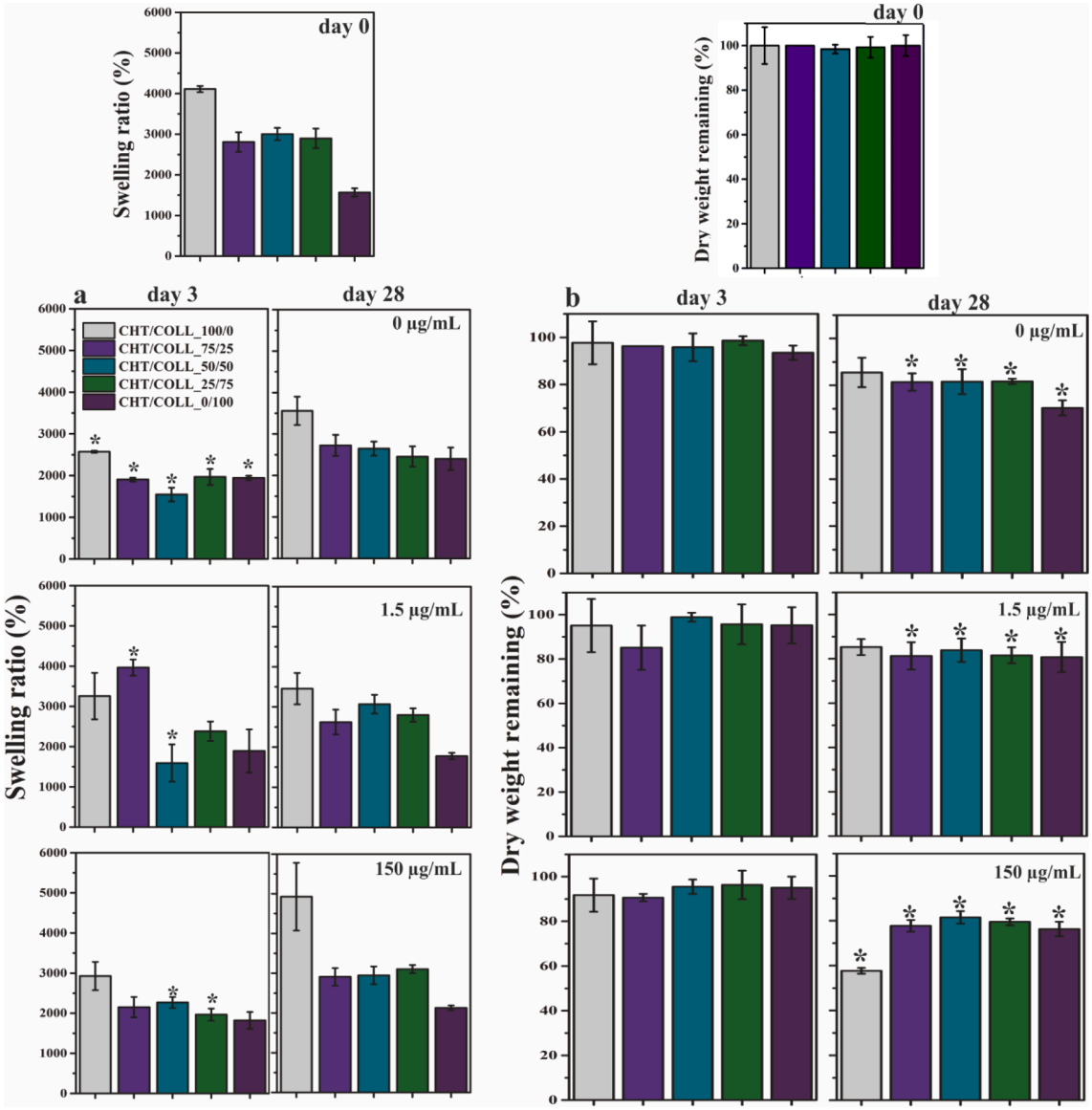

Fig. 4. In vitro degradation of chitosan/collagen scaffolds with addition of multisubstituted CaP particles. (a) Swelling ratio and (b) dry weight remaining ratio of composite scaffolds incubated in different degradation mediums at 37 °C as a function of time. Significant difference compared to scaffolds at 0 day: *($p < 0.05$).

by XRD mineralogical analysis (Fig. 2a) and FTIR spectroscopy (Fig. 2b). The XRD analysis of composite scaffolds confirmed the presence of HAp (ICDD 09–0432) in all prepared scaffolds as the single mineralogical phase. Due to Sr^{2+}, Mg^{2+}, Zn^{2+} and SeO_3^{2-} substitutions, calcium-deficient HAp was obtained and used for scaffold preparation. In addition to initially added substituents, in our previous studies [27], the presence of Na^+ ions was detected when cuttlefish bone is used as a source of Ca^{2+} ions for CaP synthesis.

The FTIR spectra of composite scaffolds was compared with that of pure collagen, chitosan and HAp to identify interactions between biopolymers and bioactive component. The pure chitosan showed the following characteristic absorption bands: (i) broad band at around 3328 cm^{-1} related to stretching of OH and NH groups, (ii) 2878 cm^{-1} corresponding to CH axial stretching, (iii) 1649 cm^{-1} corresponding to the stretching vibration of carbonyl (C = O) of amid (amide I), (iv) 1546 cm^{-1} corresponding to the amino (NH) bending of amid (amide II), (v) 1308–1427 cm^{-1} corresponding to the vibrations of OH and CH in the ring, and (vi) C–O stretching vibration of the saccharide structure is reflected in the absorption bands at 891 and broad bend around 1057 cm^{-1} [37-39]. The pure collagen showed characteristic absorption bands: (i) broad band around 3308 cm^{-1} corresponding to the stretching of NH groups coupled with hydrogen bonding (amide A) and CH stretching (amide B), (ii) 2932 and 1456 cm^{-1} corresponding to stretching vibration of CH, (iii) 1640 cm^{-1} corresponding to the C = O stretching vibration of carboxamide (amid I) functional groups along the polypeptide backbone, and (iv) 1538 and 1230 cm^{-1} related to NH bending vibrations (amide II) and CH stretching (amide III) bands [40-43]. Main characteristic bands for PO_4^{3-} groups in pure HAp structure were found at 1015 (asymmetric stretching vibration of P–O), 600 and 559 cm^{-1} (asymmetric bending vibration of O–P–O) [43]. Characteristic bands for PO_4^{3-} groups of HAp and bands for chitosan and collagen biopolymers were shifted to higher wavenumbers in composite scaffolds compared to the pure components. The shift towards higher wavenumbers indicates chemical interactions between biopolymers and HAp phase by hydrogen bonds or electrostatic interactions. The positively charged protonated amino groups of chitosan (NH_3^+) form complex with PO_4^{3-} ions and can facilitate nucleation and growth of HAp, while carbonyls can chelate Ca^{2+} ions and arrange them into a similar structure as HAp crystal [44]. In addition, the shift of characteristic bands of collagen indicate interaction between carboxylate group and nucleated

HAp crystals. Carboxylate group can bind with Ca^{2+} ions and serve as nucleation site of HAp crystals [45,46]. Homogeneously distributed nucleation sites in chitosan and collagen chains can regulate the deposition of HAp and lead to uniform distribution of mineral deposites [47].

The SEM analysis and ImageJ software were used to determine the microstructure and pore size distribution of prepared composite scaffolds (Fig. 3a). The CHT/COLL_100/0, CHT/COLL_75/25, CHT/COLL_50/50, CHT/COLL_25/75 scaffolds show a highly porous structure with open and interconnected pores, while the CHT/COLL_0/100 scaffold shows a porous structure with more closed porosity on the surface. The HAp particles are homogeneously dispersed in the chitosan/collagen matrix. Due to the not defined pores of scaffold CHT/COLL_0/100, its pore size distribution was not determined. The distribution of pore size (Fig. 3b) revealed that pore size ranged mainly from ~ 20 to 250 μm for scaffolds CHT/COLL_100/0 and CHT/COLL_25/75, and from ~ 20 to 350 μm for scaffolds CHT/COLL_50/50 and CHT/COLL_75/25. The size of the osteoblasts is in the range of 10–50 μm and the macropores with the size of 200–350 μm are considered optimal for osteoblast proliferation [48]. Macroporosity promotes osteogenesis by enhancing cell migration, cell–cell network formation, vascularization and diffusion of oxygen, nutrients and metabolic products [49,50]. In addition, micropores of < 100 μm are of great importance as they provide high surface area, enhance protein adhesion, cell seeding and attachment, cell–cell interactions, capillaries growth, vascularization and cell-matrix interactions [48-50]. Achieved porosity, pore size distribution and pore interconnectivity of the prepared scaffolds should allow cell–cell interactions, formation of vascular network and tissue formation. Vascularization of the scaffold is essential to avoid implanted-cell necrosis and the formation of acellular regions [51]. However, optimum balance between porosity, pore size distribution, biological and mechanical properties requirements is still a major challenge in the development of the scaffold. In our previous study [31], compressive strength value of 7.32 ± 0.73 kPa (70 % strain) of CHT-HAp indicated low mechanical properties implying that scaffolds can be used in small-size bone defects where there is no need for the load-bearing scaffold.

3.2. In vitro degradation analysis

Biodegradable materials are used in bone tissue engineering to allow bone tissue growth into the scaffold volume [52]. Biodegradation of porous scaffolds is a complex process that depends on various factors, such as porosity, pore size distribution, surface area, polymer type, hydrophilicity, etc., where small biomolecules produced by the degradation can regulate the regenerative microenvironment. Biopolymers are known to be less stable under degradation conditions compared to synthetic polymers. As enzymatic degradation and hydrolysis are the main degradation mechanisms of chitosan and collagen, the degradation rate under simulated biological conditions needs to be examined [52,53].

The enzymatic degradation of prepared composite scaffolds was studied at physiological conditions as a function of time (28 days) by monitoring swelling behaviour, dry weight loss, microstructure (with SEM) and thermal degradation peaks (with DSC). To distinguish between hydrolysis (dissolution) and enzymatic degradation, composite scaffolds were immersed in PBS solution without lysozyme, and with two different concentrations of lysozyme (1.5 and 150 μg/mL) to mimic the *in vivo* conditions, where the concentration of lysozyme can significantly increase in ECM from the initial concentration that is in the range 0.95–2.45 μg/mL [54]. The results shown in Fig. 4a revealed irregular changes of the swelling ratio after 3 days of incubation compared to initial water uptake at 0 day, while after 28 days of incubation there was no significant difference in swelling ratio compared to initial uptake. After 28 days of incubation, scaffold CHT/COLL_100/0 have shown the highest water uptake, while there was no significant difference in swelling ratios between degradation medium with 0, 1.5 and 150 μg/mL of lysozyme. Compared to other scaffolds, scaffold CHT/COLL_0/100 has shown the lowest initial and final water uptake in degradation medium with 1.5 and 150 μg/mL of lysozyme. As seen from Fig. 4b, after 3 days of incubation the dry weight remaining ratio did not significantly change for all scaffolds. After 28 days of incubation, the dry weight remaining ratio in different lysozyme solutions significantly decreased for all prepared scaffolds, especially for scaffold CHT/COLL_100/0 in a degradation medium with 150 μg/mL of lysozyme.

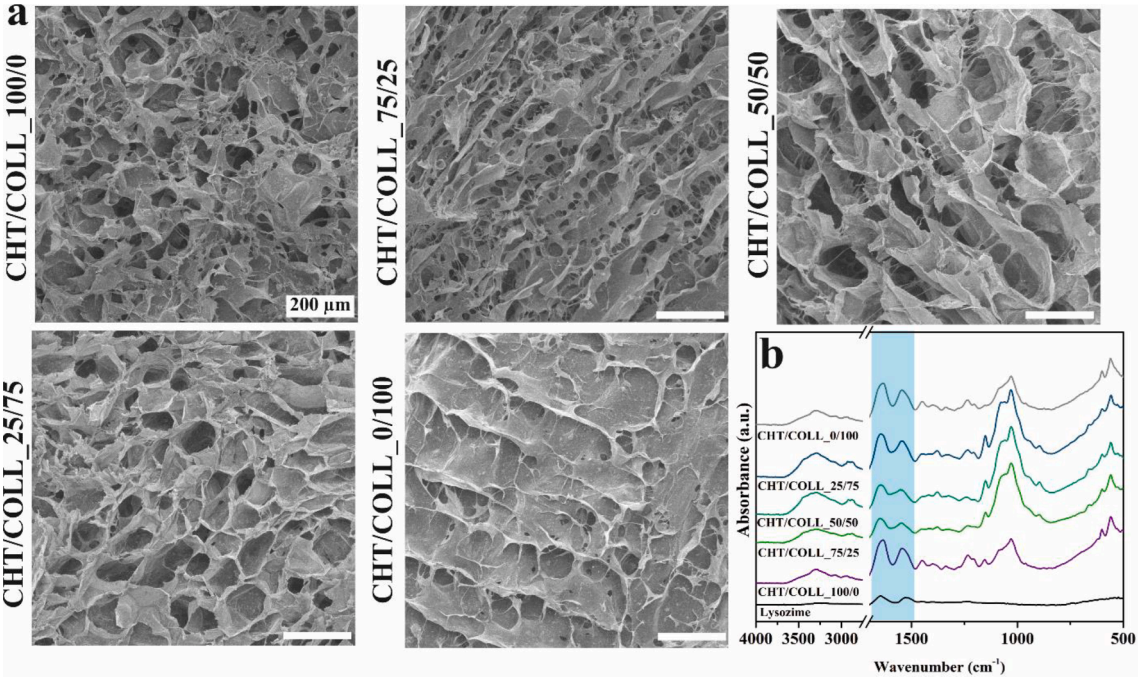

Fig. 5. Enzymatic degradation of collagen/chitosan scaffolds. (a) SEM micrographs and (b) FTIR spectra of composite scaffolds incubated in a degradation medium containing 150 μg/mL of lysozyme at 37 °C for 28 days of incubation. Lysozyme powder was used as a control in FTIR analysis.

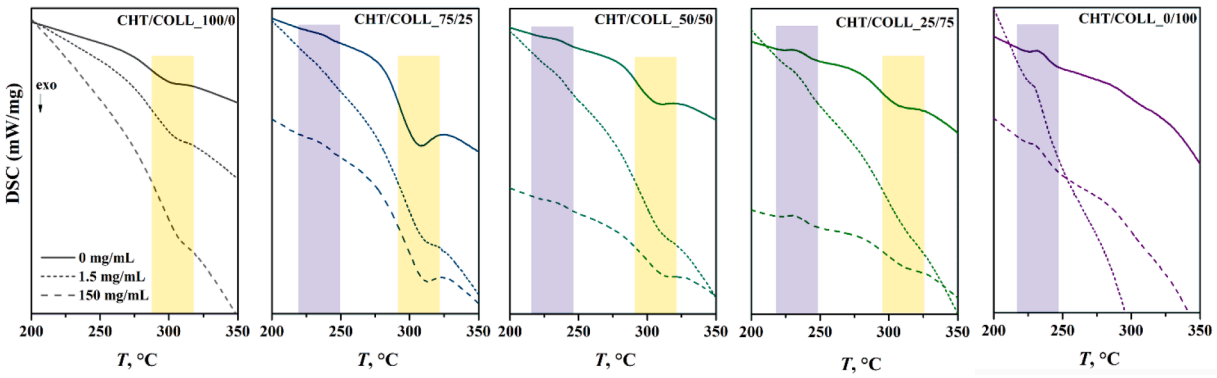

Fig. 6. Thermal degradation of incubated collagen/chitosan scaffolds. Differential scanning calorymetry curves of the prepared composite scaffolds after 28 days of incubation at 37 °C in degradation mediums with different concentrations of lysozyme. Characteristic peaks of chitosan are highlighted in yellow and the endothermic transition of collagen in purple.

Scaffold swelling capacity, structural stability and degradation rate are highly important to enable tissue formation to occur simultaneously with degradation. Swelling capacity is closely related to the pore size distribution, pore interconnectivity and biomaterials properties, playing a crucial role in cell infiltration and diffusion of oxygen, nutrients and metabolites [55,56]. Swelling is a kinetic process that involves the mass transfer and mechanical deformation and is dependent on interactions between water molecules and the carboxyl and hydroxyl groups of the polymeric network [47]. Lysozyme is a glycoside hydrolase that catalyzes the hydrolysis of β-1,4-linkages between *N*-acetylmuramic acid and *N*-acetyl-D-glucosamine residues or between *N*-acetyl-D-glucosamine residues [57]. The degradation of chitosan usually begins with the random splitting of β-1,4-glycosidic bonds (depolymerization) followed by hydrolysis of *N*-acetyl linkage (deacetylation). Consequently, molecular weight decreases and an increase in deacetylation degree is observed [58]. Degradation of chitosan leads to non-toxic variable lengths oligosaccharides formation which can be either incorporated in metabolic pathways or be excreted [52,58]. Collagen forms three polypeptide chains (α-chains) helical structures, each containing a domain characterized by the repeating motif with glycine as every third amino acid (Gly-X-Y sequences). Glycine is the smallest of all amino acids and its presence in the collagen chain is essential for the tight packing of the helical structure. The X and Y positions in the Gly-X-Y sequences can represent any amino acid other than glycine, most frequently proline and hydroxyproline. The tightly packed helical structure of fibrillar collagens makes them highly resilient to degradation. Only a few proteases have been identified as capable of degrading fibrillar collagen, including the cysteine protease cathepsin K and members of the matrix metalloproteinase family. However, certain collagens can be degraded by lysosomal cysteine proteases *in vivo* [59]. The inhibition of degradation in a degradation medium with 150 μg/mL of lysozyme for a scaffold containing collagen is in agreement with the study by Zulkifli et al. [60] where hydroxyethyl cellulose/poly(vinyl) alcohol/collagen scaffold showed a slower degradation rate in PBS as compared to the scaffold without collagen. Thus, the slower degradation rate of collagen incorporated hydroxyethyl cellulose/poly(vinyl) alcohol in PBS buffer solution might be due to the difficulty of hydrolyzing the peptide bond in a neutral medium [60]. The slower degradation rate of composite CHT/COLL/CaP scaffolds compared to the chitosan-based scaffold in a degradation medium with 150 μg/mL of lysozyme can be due to lower or lack of activity of lysozyme towards collagen. However, the similar stability of composite scaffolds CHT/COLL_75/25, CHT/COLL_50/50, CHT/COLL_25/75 can be explained by interactions between chitosan and collagen chains where several types of interactions are possible. The side groups and the end groups –COOH and NH_2 in the collagen chain are capable of forming hydrogen bonds with –OH and NH_2 groups in chitosan.The long chain of chitosan can wind around the collagen triple helix and the entanglement of two different macromolecules may form a complex that can lead to higher stability under physiological conditions. In addition, as chitosan and collagen were mixed in acidic conditions, they may be bonded ionically due to oppositely charged ionic polymers, particularly the cationic polysaccharide chitosan (NH_3^+) and anionic $-COO^-$ group in collagen, leading to higher composite stability [61].

In Fig. 5a, the microstructures of the prepared composite scaffolds after 28 days of incubation at 37 °C (lysozyme concentration 150 μg/mL) did not show a significant difference to the initial scaffolds (Fig. 3). The highly porous structure, with open porosity, has been retained after 28 days of enzymatic degradation in all scaffolds expect in the scaffold CHT/COLL_0/100 where a structure without surface pores was also initially observed. The open porous structure is crucial for the uniform degradation of scaffolds, cell seeding and migration, vascularization, and diffusion of nutrients, oxygen and metabolic waste through the entire scaffold volume. Even if naturally derived polymers typically are not highly stable during longer periods under degradation conditions, all the prepared scaffolds have shown high stability during 28 days despite the significant decrease of scaffold weights in different degradation mediums.

The FTIR spectra (Fig. 5b) of composite scaffolds after 28 days of incubation at 37 °C (lysozyme concentration 150 μg/mL) have shown all characteristic bands for chitosan, collagen and HAp phases as determined in Fig. 2b. The absorption bands at 1647 and 1523 cm^{-1}, characteristic for lysozyme amide I (C = O) and amide II (NH) of the polypeptide chain, are evident in all samples incubated in degradation

Table 2
Peak temperatures (°C) of the chitosan exotherms and transition temperatures of collagen in dependence of the lysozyme concentrations.

	Temperature (°C)									
	CHT/COLL_100/0		CHT/COLL_75/25		CHT/COLL_50/50		CHT/COLL_25/75		CHT/COLL_0/100	
L (μg/mL)	CHT	COLL	CHT	COLL	CHT	COLL	CHT	COLL	CHT	COLL
0	300.2	–	308.4	236.2	306.4	235.0	307.8	233.7	–	233.2
1.5	302.1	–	309.9	238.4	308.2	233.1	309.2	232.9	–	231.5
150	304.9	–	311.6	238.8	311.0	228.9	310.3	229.6	–	229.7

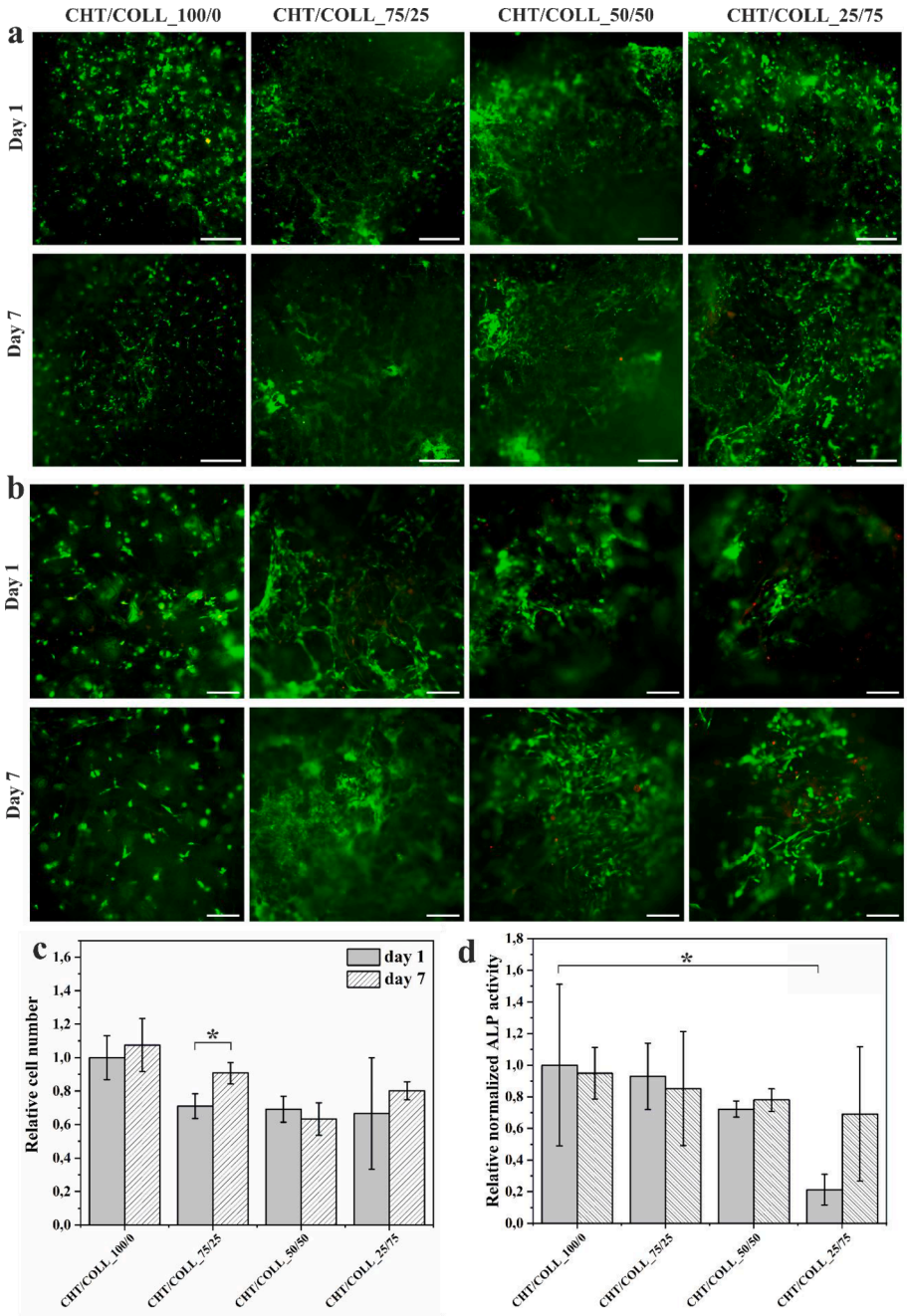

Fig. 7. Biological characterization of collagen/chitosan scaffolds. (a, b) Qualitative and (c) quantitative analysis of seeded hBMSC after 1 and 7 days of cell culture obtained by live dead and CyQUANT assay, respectively. Live cells are stained in green; dead cells are stained in red. (d) ALP activity normalized to the cell amount. Scale bar: 500 μm. Significant difference: *($p < 0.05$).

medium with lysozyme. Even though the samples were washed several times after the incubation with demineralized water, the characteristic absorption bands are evident due to strong attractive electrostatic interactions between the biopolymers and lysozyme that are essential for glycoside bond cleavage [62].

DSC results of the prepared scaffolds after 28 days of incubation at 37 °C in PBS with two different lysozyme concentrations (1.5 and 150 μg/mL) are shown in Fig. 6. Pure chitosan CHT/COLL_100/0 scaffold degraded at ~ 300 °C giving an exothermic peak and similar peaks originating from chitosan degradation were observed in CHT/COLL_75/25, CHT/COLL_50/50 and CHT/COLL_25/75 scaffolds with shifts of 1–2 °C to higher temperatures (Table 2) with increasing lysozyme concentration. Moreover, the addition of collagen to the scaffolds resulted in the exothermic peak shift of about 7 – 8 °C to higher temperatures in comparison to the pure chitosan CHT/COLL_100/0 scaffold. The CHT/COLL_0/100 scaffold showed an endothermic peak/transition at ~ 230 °C. This endothermic transition was observed in scaffolds CHT/COLL_75/25, CHT/COLL_50/50 and CHT/COLL_25/75 as well, and a shift of this transition towards lower temperatures, with increasing lysozyme concentration (Table 2), was observed.

The scaffolds prepared from natural polymers often degrade rapidly which is difficult to control under physiological conditions. Therefore, insight into the structural stability and degradation rate is of great importance to allow tissue formation which occurs simultaneously with the degradation process [63]. The endothermic transition observed at ~ 230 °C was attributed to the denaturation of dry collagen and corresponds to the helix-coil transition caused by thermal disruption of hydrogen bonds [64,65], while degradation of chitosan is an exothermic

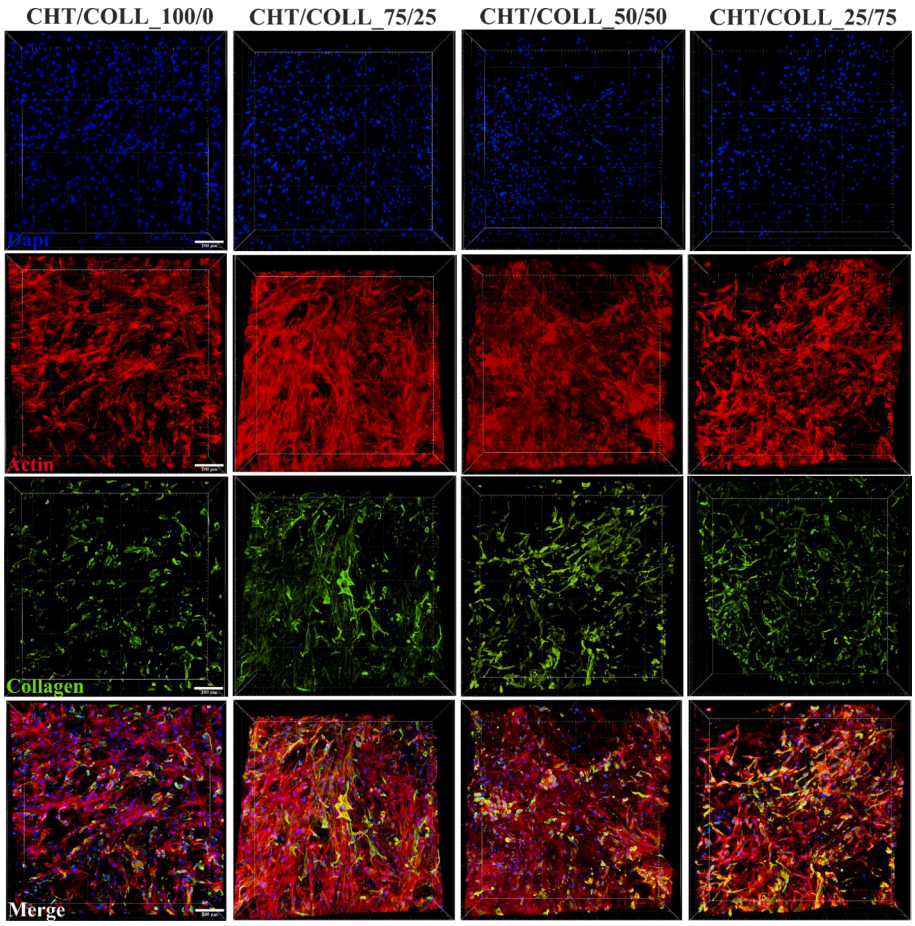

Fig. 8. The production of type I collagen on the hBMSC-seeded chitosan/collagen scaffolds, containing multi-substituted CaP particles, after 14 days of cell culture. Cell nuclei stained with DAPI (blue), actin cytoskeleton stained with phalloidin (red) and an antibody for human type I collagen (green). Scale bar: 200 μm.

process that gave characteristic peaks in the 300 – 312 °C range. Under physiological conditions, chitosan degrades *via* hydrolysis by breaking its polymer network into smaller chains, whereby the chain scission of β-1–4 *N*-acetyl glucosamine is mainly caused by lysozymes as explained in our previous studies [22,66]. Despite expectations that degradation of chitosan would result in the exothermic peak shift towards lower temperatures due to the chain scissions leading to the lower molecular weights, analyzed scaffolds have shown different behaviour. The observed exothermic peaks of the scaffolds were shifted towards higher temperatures which can be explained by the chitosan-collagen interactions [67]. Since the degradation results in a large number of smaller chitosan chains, electrostatic interactions take place resulting in the formation of hydrogen bonds between chitosan and collagen chains [67,68].

3.3. Biological characterization

The *live/dead* assay shows homogeneously dispersed hBMSCs with good viability and cell–cell interactions after 1 and 7 days of cell culture for all the scaffolds (Fig. 7a and 7b). CHT/COLL_0/100 was excluded from biological characterization because it did not show desired highly porous structure with an appropriate pore size distribution, essential for migration of seeded cells into the scaffold. The shape of the cells was more elongated on scaffolds containing collagen compared to scaffold CHT/COLL_100/0 without collagen, where the cells were more spherical.

The number of cells (Fig. 7c) was similar between scaffolds CHT/COLL_75/25, CHT/COLL_50/50 and CHT/COLL_25/75, while higher amount of the cells were present in scaffold CHT/COLL_100/0. No significant difference was observed between days 1 and 7 for prepared scaffolds except for scaffold CHT/COLL_75/25 where a significant increase after 7 days of cell culture is observed. ALP acts as an early indicator of cellular activity and differentiation and is the first functional gene expressed in the process of calcification mechanism [69,70]. ALP activity normalized to the cell number (Fig. 7d) was similar for scaffolds CHT/COLL_100/0, CHT/COLL_75/25 and CHT/COLL_50/50. No significant difference in normalized ALP activity was observed between prepared scaffolds, except a statistically lower ALP activity for scaffolds CHT/COLL_25/75 at 1 day of cell culture, compared to scaffold CHT/COLL_100/0. The bone mineralization process starts with HAp crystals formation in the matrix cavities and distribution in the ECM. Further, HAp crystals are infiltrated in the matrix vessel membrane and expanded into the extracellular area. Pyrophosphate is an inhibitor of HAp formation and it is produced by nucleotide pyrophosphatase phosphodiesterase 1 from nucleotide triphosphates. In the second stage of mineralization, ALP plays a crucial role in the hydrolysis of pyrophosphate to phosphate, maintaining their ratio level suitable for HAp formation [71].

The pore size distribution in the scaffold significantly affects cellular activity and even small changes in pore size can greatly affect cell adhesion and cell–cell interactions [72]. Previous studies indicated that a pore size distribution in the range of 96–150 μm is optimal for cell attachment, while other studies have shown a need for large pores in the range of 300–800 μm for successful bone growth in scaffolds [73]. According to Murphy et al. [72] small pores may have a beneficial effect on initial cell adhesion but ultimately the improved cellular infiltration provided by scaffolds with larger pores outweighs this effect and suggests that scaffolds with larger pores might be optimal for bone tissue

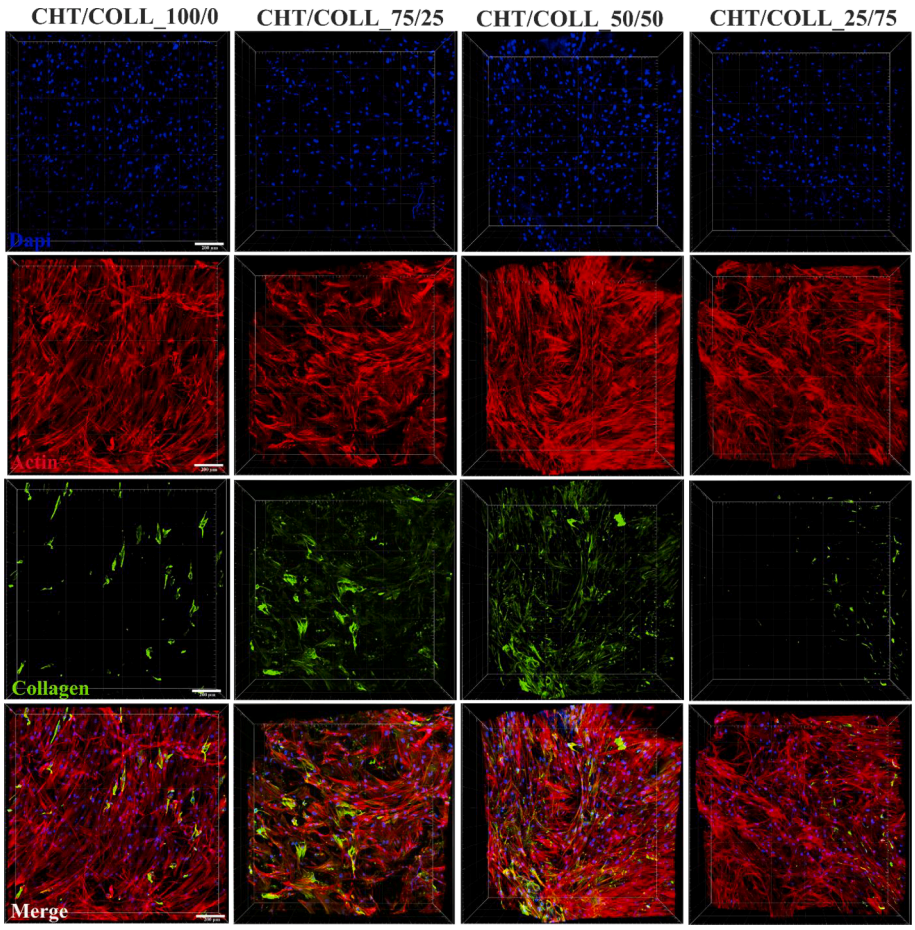

Fig. 9. The production of type I collagen on the hBMSC-seeded chitosan/collagen scaffolds, containing multi-substituted CaP particles, after 21 days of cell culture. Cell nuclei stained with DAPI (blue), actin cytoskeleton stained with phalloidin (red) and an antibody for human type I collagen (green). Scale bar: 200 μm.

repair [73]. According to Mao et al. [74], expression of ALP increased only in cells with both, direct contact with neighboring cells and adhesion to stiffer substrates, indicating the important role of cell–cell interaction in ALP expression and bone regeneration.

Along with ALP activity quantification, osteogenic differentiation of hBMSCs seeded on the scaffolds was qualitatively determined by analysing the presence of type I collagen at 14 (Fig. 8) and 21 (Fig. 9) days of cell culture by using confocal fluorescence microscopy. Cell nuclei stained with DAPI appeared in blue, actin cytoskeleton in red, and type I collagen in green. Type I collagen expression was found at 14 and 21 days of cell culture, implying the good osteogenic potential of prepared composite scaffolds. Immunocytochemical staining showed homogeneous type I collagen production within prepared scaffolds, except for scaffold CHT/COLL_25/75 where type I collagen expression was diminished after 21 days of cell culture. Higher production of type I collagen is evident for scaffolds CHT/COLL_75/25 and CHT/COLL_50/50 after both, 14 and 21 days of cell culture. In all prepared scaffolds, high cytoskeleton interconnectivity is evident implying good cell–cell interactions, essential for the bone regeneration process. The videos of confocal fluorescence microscopy are attached in Video S1 of supplementary information.

The process of osteogenesis is directed by connected biological processes initiated by the recruitment of MSCs to bone remodeling sites and subsequent proliferation, lineage commitment, expression of lineage-specific markers, collagen secretion, and ECM mineralization [75]. Type I collagen is one of the most important organic components of ECM and therefore the analysis of cells' potential to secrete type I collagen in scaffolds is important for potential bone tissue engineering applications [9]. In the current study, we hypothesize that the addition of type I collagen in the scaffolds based on chitosan and Mg, Se, Sr, Zn-substituted CaPs will have a positive effect on the osteogenic properties of the scaffolds. The addition of 25% and 50% of the type I collagen within the chitosan matrix enhanced cytoskeletal organization, cell-matrix interactions and type I collagen production of hBMSCs. Scaffold CHT/COLL_75/25 showed similar cell numbers and ALP expression as scaffold CHT/COLL_100/0, with enhanced type I collagen production.

In natural bone tissue, collagen fibers are the template for the mineralization and make an important contribution to bone formation and the bone remodeling process. Therefore, collagen has been widely explored as a biomaterial for bone defect regeneration. However, pure collagen implants have limitations in the bone regeneration process due to their limited osteoinductivity [76]. Even though pure collagen matrix mimics natural bone environment, combination with other bioactive components can lead to improved properties of the composite scaffold as a whole. Chitosan and collagen mixtures with different additives are widely explored for applications in tissue engineering [77]. In a recent study by Karakeçili et al. [78], chitosan/collagen/HAp composite scaffolds with 0, 20 and 50 wt% of collagen and 1 wt% of HAp were prepared. Scaffolds with the highest collagen content showed the best biological properties. However, when different bioactive additives are used within chitosan/collagen blends, a wide range of polymer compositions should be explored as it might lead to different scaffold properties and affect the overall scaffold physiochemical and biological properties. Different compositions of polymer phases within the scaffolds lead to different polymer interactions and can affect the ion release from the inorganic phase. Therefore, a wide range of collagen was explored in this study to determine adequate composition when multi-substituted HAp is used as an inorganic additive. Based on the

performed characterization, it can be concluded that scaffold CHT/COLL_75/25 has provided a suitable environment for enhanced osteogenesis. Regarding future work on this topic, *in vitro* studies for late osteogenic markers and *in vivo* studies on animal model need to be performed to examine late osteogenesis and biodegradation to confirm the applicability of the scaffold CHT/COLL_75/25 for bone tissue engineering applications.

4. Conclusions

The present research shows that the addition of type I collagen in composite scaffolds based on chitosan and multi-substituted HAp increased scaffold stability under physiological and enzymatic conditions, even when natural polymers were used. The addition of collagen within the chitosan matrix, containing multi-substituted HAp, did not influence the scaffold microstructure and CHT/COLL_100/0, CHT/COLL_75/25, CHT/COLL_50/50, CHT/COLL_25/75 scaffolds act as three-dimensional support for hBMSCs proliferation and differentiation into osteoblasts. The addition of 25 % of type I collagen into the chitosan matrix led to desired cell proliferation and morphology, cell–cell interactions, and the production of type I collagen by hBMSC, as shown by confocal fluorescence microscopy. Despite good osteoinductive properties, poor mechanical properties associated with porous biopolymer scaffolds remain one of the main challenges to applying these materials in bone tissue engineering. Future studies will be focused on analysis and increasing the mechanical performance of studied materials with the best osteogenic properties. To meet requirements, the CHT/COLL_75/25 will be combined with the highly porous HAp construct fabricated by ceramic stereolithography as an additive manufacturing method.

5. Data availability statement

The data that support the findings of this study are available from the corresponding author upon reasonable request.

Declaration of Competing Interest

The authors declare that they have no known competing financial interests or personal relationships that could have appeared to influence the work reported in this paper.

Data availability

Data will be made available on request.

Acknowledgements

The financial support of the European Regional Development Fund (grant KK.01.1.1.07.0014) is gratefully acknowledged. This work has been supported in part by the Virtulab project (KK.01.1.1.02.0022), co-funded by the European Regional Development Fund. Tampere University Research Centre of Science Mimicking Life, Tampere Imaging Facility (TIF), and Cell Tech Laboratories of Tampere University are gratefully acknowledged. The authors thank Anna-Maija Honkala and Sari Kalliokoski for their excellent technical assistance.

Appendix A. Supplementary data

Supplementary data to this article can be found online at https://doi.org/10.1016/j.eurpolymj.2023.112129.

References

[1] H. Lin, J. Sohn, H. Shen, M.T. Langhans, R.S. Tuan, Bone marrow mesenchymal stem cells: Aging and tissue engineering applications to enhance bone healing, Biomaterials 203 (2019) 96–110, https://doi.org/10.1016/j.biomaterials.2018.06.026.

[2] G. Zhu, T. Zhang, M. Chen, K. Yao, X. Huang, B. Zhang, Y. Li, J. Liu, Y. Wang, Z. Zhao, Bone physiological microenviroment and healing mechanism: basis for future bone-tissue engineering scaffolds, Bioact. Mater. 6 (2021) 4110–4140, https://doi.org/10.1016/j.bioactmat.2021.03.043.

[3] E. Hernlund, A. Svedbom, M. Ivergård, J. Compston, C. Cooper, J. Stenmark, E. V. McCloskey, B. Jonsson, J.A. Kanis, Osteoporosis in the European union: medical management, epidemiology and economic burden. A report prepared in collaboration with the international osteoporosis foundation (IOF) and the European federation of pharmaceutical industry associations (EFPIA), Arch Osteoporos 8 (2013) 136, https://doi.org/10.1007/s11657-013-0136-1.

[4] I. Sallent, H. Capella-Monsonís, P. Procter, I.Y. Bozo, R.V. Deev, D. Zubov, R. Vasyliev, G. Perale, G. Pertici, J. Baker, P. Gingras, Y. Bayon, D.I. Zeugolis, The Few Who Made It: Commercially and Clinically Successful Innovative Bone Grafts, Front Bioeng. Biotechnol. 8 (2020) 952, https://doi.org/10.3389/fbioe.2020.00952.

[5] S. Vukicevic, H. Oppermann, D. Verbanac, M. Jankolija, I. Popek, J. Curak, J. Brkljacic, M. Pauk, I. Erjavec, I. Francetic, I. Dumic-Cule, M. Jelic, D. Durdevic, T. Vlahovic, R. Novak, V. Kufner, T. Bordukalo Niksic, M. Kozlovic, Z. Banic Tomisic, J. Bubic-Spoljar, I. Bastalic, S. Vikic-Topic, M. Peric, M. Pecina, L. Grgurevic, The clinical use of bone morphogenetic proteins revisited: a novel biocompatible carrier device OSTEOGROW for bone healing, Intern. Orthopaed. 38 (2014) 635–647, https://doi.org/10.1007/s00264-013-2201-1.

[6] S. Bose, G. Fielding, S. Tarafder, A. Bandyopadhyay, Understanding of dopant induced osteogenesis and angiogenesis in calcium phosphate ceramics, Trends Biotechnol. 31 (2013) 594–605, https://doi.org/10.1016/j.tibtech.2013.06.005.

[7] J.A. Inzana, D. Olvera, S.M. Fuller, J.P. Kelly, O.A. Graeve, E.M. Schwarz, S. L. Kates, H.A. Awad, 3D printing of composite calcium phosphate and collagen scaffolds for bone regeneration, Biomaterials 35 (2014) 4026–4034, https://doi.org/10.1016/j.biomaterials.2014.01.064.

[8] M. Sadat-Shojai, M.T. Khorasani, E. Dinpanah-Khoshdargi, A. Jamshidi, Synthesis methods for nanosized hydroxyapatite with diverse structures, Acta Biomater. 9 (2013) 7591–7621, https://doi.org/10.1016/j.actbio.2013.04.012.

[9] B. Safari, S. Davaran, A. Aghanejad, Osteogenic potential of the growth factors and bioactive molecules in bone regeneration, Int. J. Biol. Macromol. 175 (2021) 544–557, https://doi.org/10.1016/j.ijbiomac.2021.02.052.

[10] D. Zhang, X. Wu, J. Chen, K. Lin, The development of collagen based composite scaffolds for bone regeneration, Bioact. Mater. 3 (2018) 129–138, https://doi.org/10.1016/j.bioactmat.2017.08.004.

[11] L. Guo, Z. Liang, L. Yang, W. Du, T. Yu, H. Tang, C. Li, H. Qiu, The role of natural polymers in bone tissue engineering, J Control Release. 338 (2021) 571–582, https://doi.org/10.1016/j.jconrel.2021.08.055.

[12] P.C. Pires, F. Mascarenhas-Melo, K. Pedrosa, D. Lopes, J. Lopes, A. Macario-Soares, D. Peixoto, P.S. Giram, F. Veiga, A.C. Paiva-Santos, Polymer-based biomaterials for pharmaceutical and biomedical applications: A focus on topical drug administration, Eur. Polym. J. 187 (2023), 111868, https://doi.org/10.1016/j.eurpolymj.2023.111868.

[13] T. Cordonnier, J. Sohier, P. Rosset, P. Layrolle, Biomimetic Materials for Bone Tissue Engineering—State of the Art and Future Trends, Adv. Eng. Mater. 13 (2011) B135–B150, https://doi.org/10.1002/adem.201080098.

[14] H. Tan, C.R. Chu, K.A. Payne, K.G. Marra, Injectable in situ forming biodegradable chitosan-hyaluronic acid based hydrogels for cartilage tissue engineering, Biomaterials 30 (2009) 2499–2506, https://doi.org/10.1016/j.biomaterials.2008.12.080.

[15] R. Mansouri, Y. Jouan, E. Hay, C. Blin-Wakkach, A. Ostertag, C. Le Henaff, C. Marty, V. Geoffroy, P.J. Marie, M. Cohen-Solal, D. Modrowski, Osteoblastic heparan sulfate glycosaminoglycans control bone remodeling by regulating Wnt signaling and the crosstalk between bone surface and marrow cells, Cell Death Dis. 8 (2017) e2902.

[16] S. Islam, M.A.R. Bhuiyan, M.N. Islam, Chitin and Chitosan: Structure, Properties and Applications in Biomedical Engineering, J. Polym. Environ. 25 (2017) 854–866.

[17] L. Roshini Yadav, S. VijiChandran, K. Lavanya, N. Selvamurugan, Chitosan-based 3D-printed scaffolds for bone tissue engineering, Int. J. Biol. Macromol. 183 (2021) 1925–1938, https://doi.org/10.1016/j.ijbiomac.2021.05.215.

[18] I. Fasolino, M.G. Raucci, A. Soriente, C. Demitri, M. Madaghiele, A. Sannino, L. Ambrosio, Osteoinductive and anti-inflammatory properties of chitosan-based scaffolds for bone regeneration, Mater. Sci. Eng. C 105 (2019), 110046, https://doi.org/10.1016/j.msec.2019.110046.

[19] A.E. Erickson, J. Sun, S.K. Lan Levengood, S. Swanson, F.C. Chang, C.T. Tsao, M. Zhang, Chitosan-based composite bilayer scaffold as an in vitro osteochondral defect regeneration model, Biomed. Microdevices 21 (2019) 34, https://doi.org/10.1007/s10544-019-0373-1.

[20] J.A. Lett, S. Sagadevan, I. Fatimah, M.E. Hoque, Y. Lokanathan, E. Leonard, S. F. Alshahateet, R. Schirhagal, W. Chun Oh, Recent advances in natural polymer-based hydroxyapatite scaffolds: Properties and applications, Eur. Polym. J. 148 (2021), 110360, https://doi.org/10.1016/j.eurpolymj.2021.110360.

[21] G.A. Rico-Llanos, S. Borrego-González, M. Moncayo-Donoso, J. Becerra, R. Visser, Collagen Type I Biomaterials as Scaffolds for Bone Tissue Engineering, Polymers 13 (2021) 599, https://doi.org/10.3390/polym13040599.

[22] A. Ressler, M. Antunović, L. Teruel-Biosca, G. Gallego Ferrer, S. Babić, I. Urlić, M. Ivanković, H. Ivanković, Osteogenic differentiation of human mesenchymal stem cells on substituted calcium phosphate/chitosan composite scaffold, Carbohydr. Polym. 277 (2022), 118883, https://doi.org/10.1016/j.carbpol.2021.118883.

[23] S. Chen, Y. Shi, X. Zhang, J. Ma, Biomimetic synthesis of Mg-substituted hydroxyapatite nanocomposites and three-dimensional printing of composite scaffolds for bone regeneration, J. Biomed. Mater. Res. 107 (2019) 2512–2521, https://doi.org/10.1002/jbm.a.36757.
[24] A. Farzadi, F. Bakhshi, M. Solati-Hashjin, M. Asadi-Eydivand, N.A. abu Osman Magnesium incorporated hydroxyapatite: synthesis and structural properties characterization, Ceram. Int. 40 (2014) 6021–6029, https://doi.org/10.1016/j.ceramint.2013.11.051.
[25] I. Cacciotti, A. Bianco, M. Lombardi, L., Montanaro Mg-substituted hydroxyapatite nanopowders: synthesis, thermal stability and sintering behaviour, J. Eur. Ceram. 29 (2009) 2969–2978, https://doi.org/10.1016/j.jeurceramsoc.2009.04.038.
[26] K. Pajor, L. Pajchel, B. Kolodziejska, J. Kolmas, Selenium-Doped hydroxyapatite nanocrystals-synthesis, physicochemical properties and biological significance, Crystals 8 (2018) 188, https://doi.org/10.3390/cryst8050188.
[27] A. Ressler, M. Antunović, M. Cvetnić, M. Ivanković, H. Ivanković, Selenite substituted calcium phosphates: preparation, characterization, and cytotoxic activity, Materials 14 (2021) 3436, https://doi.org/10.3390/ma14123436.
[28] L. Stipniece, S. Wilson, J.M. Curran, R. Chen, K. Salma-Ancane, P.K. Sharma, B. J. Meenan, A.R. Boyd, Strontium substituted hydroxyapatite promotes direct primary human osteoblasts maturation, Ceram. Int. 47 (2021) 3368–3379, https://doi.org/10.1016/j.ceramint.2020.09.182.
[29] A. Ressler, M. Cvetnić, M. Antunović, I. Marijanović, M. Ivanković, H. Ivanković, Strontium substituted biomimetic calcium phosphate system derived from cuttlefish bone, J. Biomed. Mater. Res. B Appl. Biomater. 18 (2019) 1697–1709, https://doi.org/10.1002/jbm.b.34515.
[30] A. Ressler, T. Ivanković, I. Ivanišević, M. Cvetnić, M. Antunović, I. Urlić, H. Ivanković, M. Ivanković, Multiphase zinc and magnesium mono-substituted calcium phosphates derived from cuttlefish bone: A multifunctional biomaterials, Ceram. Int. 49 (2023) 11005–11017, https://doi.org/10.1016/j.ceramint.2022.11.295.
[31] A. Rogina, P. Rico, G. Gallego-Ferrer, M. Ivanković, H. Ivanković, In Situ Hydroxyapatite Content Affects the Cell Differentiation on Porous Chitosan/Hydroxyapatite Scaffolds, Ann Biomed Eng. 44 (2016) 1107–1119, https://doi.org/10.1007/s10439-015-1418-0.
[32] B. Porstmann, K. Jung, H. Schmechta, U. Evers, M. Pergande, T. Porstmann, H. J. Kramm, H. Krause, Measurement of lysozyme in human body fluids: Comparison of various enzyme immunoassay techniques and their diagnostic application, Clin. Biochem. 22 (1989) 349–355, https://doi.org/10.1016/s0009-9120(89)80031-1.
[33] A. Gebraad, R. Kornilov, S. Kaur, S. Miettinen, S. Haimi, H. Peltoniemi, B. Mannerström, R. Seppänen-Kaijansinkko, Monocyte-derived extracellular vesicles stimulate cytokine secretion and gene expression of matrix metalloproteinases by mesenchymal stem/stromal cells, FEBS J. 285 (2018) 2337–2359, https://doi.org/10.1111/febs.14485.
[34] L. Tirkkonen, S. Haimi, S. Huttunen, J. Wolff, E. Pirhonen, G.K. Sándor, S. Miettinen, Osteogenic medium is superior to growth factors in differentiation of human adipose stem cells towards bone-forming cells in 3D culture, Eur Cell Mater. 25 (2013) 144–158, https://doi.org/10.22203/ecm.v025a10.
[35] A. Palmroth, S. Pitkänen, M. Hannula, K. Paakinaho, J. Hyttinen, S. Miettinen, M. Kellomäki, Evaluation of scaffold microstructure and comparison of cell seeding methods using micro-computed tomography-based tools, J. R. Soc. Interface 17 (2020) 20200102, https://doi.org/10.1098/rsif.2020.0102.
[36] M. Ojansivu, S. Vanhatupa, L. Björkvik, H. Häkkänen, M. Kellomäki, R. Autio, J. A. Ihalainen, L. Hupa, S. Miettinen, Bioactive glass ions as strong enhancers of osteogenic differentiation in human adipose stem cells, Acta Biomat. 21 (2015) 190–203, https://doi.org/10.1016/j.actbio.2015.04.017.
[37] H.F.G. Barbosa, D.S. Francisco, A.P.G. Ferreira, É.T.G. Cavalheiro, A new look towards the thermal decomposition of chitins and chitosans with different degrees of deacetylation by coupled TG-FTIR, Carbohydr Polym. 225 (2019), 115232, https://doi.org/10.1016/j.carbpol.2019.115232.
[38] Y. Yuang, W. Tan, J. Zhang, Q. Li, Z. Guo, Water-soluble amino functionalized chitosan: Preparation, characterization, antioxidant and antibacterial activities, Int. J. Biol. Macromol. 217 (2022) 969–978, https://doi.org/10.1016/j.ijbiomac.2022.07.187.
[39] Z. Zhang, Z. Zhong, Z. Zhao, Preparation, characterization and antimicrobial activities of cyclic substituted chitosan derivatives, Int. J. Biol. Macromol. 193 (2021) 474–480, https://doi.org/10.1016/j.ijbiomac.2021.10.101.
[40] F. Fahimipour, E. Dashtimoghadam, M. Rasoulianboroujeni, M. Yazdimamaghani, K. Khoshroo, M. Tahriri, A. Yadegari, J.A. Gonzalez, D. Vashaee, D.C. Lobner, T. S. Jafarzadeh Kashi, L. Tayebi, Collagenous matrix supported by a 3D-printed scaffold for osteogenic differentiation of dental pulp cells, Dent. Mater. 34 (2018) 209–220, https://doi.org/10.1016/j.dental.2017.10.001.
[41] H. Goel, N. Gupta, D. Santhiya, N. Dey, H.B. Bohidar, A. Bhattacharya, Bioactivity reinforced surface patch bound collagen-pectin hydrogel, Int. J. Biol. Macromol. 174 (2021) 240–253, https://doi.org/10.1016/j.ijbiomac.2021.01.166.
[42] T. Riaz, R. Zeeshan, F. Zarif, K. Ilyas, N. Muhammad, S.Z. Safi, A. Rahim, S.A. A. Rizvi, I.U. Rehman, FTIR analysis of natural and synthetic collagen, Appl. Spectrosc. Rev. 53 (2018) 703–746, https://doi.org/10.1080/05704928.2018.1426595.
[43] F. Wenpo, L. Gaofeng, F. Shuying, Q. Yuanming, T. Keyong, Preparation and characterization of collagen-hydroxyapatite/pectin composite, Int. J. Biol. Macromol. 74 (2015) 218–223, https://doi.org/10.1016/j.ijbiomac.2014.11.031.
[44] A. Rogina, P. Rico, G. Gallego Ferrer, M. Ivankovic, H. Ivankovic, In Situ Hydroxyapatite Content Affects the Cell Differentiation on Porous Chitosan/Hydroxyapatite Scaffolds, Ann. Biomed. Eng. 44 (2016) 1107–1119, https://doi.org/10.1007/s10439-015-1418-0.
[45] S.H. Rhee, J.D. Lee, Nucleation of Hydroxyapatite Crystal throughChemical Interaction with Collagen, J. Am. Ceram. Soc. 83 (2000) 2890–2892.
[46] A. Ficai, E. Andronescu, G. Voicu, C. Ghitulica, B.S. Vasile, D. Ficai, V. Trandafir, Self-assembled collagen/hydroxyapatite composite materials, Chem. Enf. J. 160 (2010) 794–800, https://doi.org/10.1016/j.cej.2010.03.088.
[47] A. Hassani, A.B. Khoshfetrat, R. Rahbarghazi, S. Saki, Collagen and nano-hydroxyapatite interactions in alginate-based microcapsule provide an appropriate osteogenic microenvironment for modular bone tissue formation, Carbohydr. Polym. 277 (2022), 118807, https://doi.org/10.1016/j.carbpol.2021.118807.
[48] N. Abbasi, S. Hamlet, R.M. Love, N.T. Nguyen, Porous scaffolds for bone regeneration, J. Sci.: Adv. Mater. Devices 5 (2020) 1–9, https://doi.org/10.1016/j.jsamd.2020.01.007.
[49] P. Deb, A.B. Deoghare, A. Borah, E. Barua, S. Das Lala, Scaffold development using biomaterials: a review, Mater. Today: Proc. 5 (2018) 12909–112191, https://doi.org/10.1016/j.matpr.2018.02.276.
[50] M.A. Fernandez-Yague, S.A. Abbah, L. McNamara, D.I. Zeugolis, A. Pandit, M. J. Biggs, Biomimetic approaches in bone tissue engineering: Integrating biological and physicomechanical strategies, Adv. Drug Deliv. Rev. 84 (2015) 1–29, https://doi.org/10.1016/j.addr.2014.09.005.
[51] T. Cardonnier, J. Sohier, P. Rosset, P. Layrolle, Biomimetic Materials for Bone Tissue Engineering - State of the Art and Future Trends, Adv. Eng. Mater. 13 (2011) 135–150, https://doi.org/10.1002/adem.201080098.
[52] S. Wei, J.X. Ma, L. Xu, X.S. Gu, X.L. Ma, Biodegradable materials for bone defect repair, Military Med. Res. 7 (2020) 54, https://doi.org/10.1186/s40779-020-00280-6.
[53] K. Kalantari, A.M. Afifi, H. Jahangirian, T.J. Webster, Biomedical applications of chitosan electrospun nanofibers as a green polymer - Review, Carbohydr. Polym. 207 (2019) 588–600, https://doi.org/10.1016/j.carbpol.2018.12.011.
[54] Y.P. Hou, J.L. Hu, H. Park, M. Lee, Chitosan-based nanoparticles as a sustained protein release carrier for tissue engineering applications, J. Biomed. Mater. Res. A 100 (2012) 939–944, https://doi.org/10.1002/jbm.a.34031.
[55] F.F. Azhar, A. Olad, R. Salehi, Fabrication and characterization of chitosan-gelatin/nanohydroxyapatite-polyaniline composite with potential application in tissue engineering scaffolds, Des. Monomers Polym. 17 (2014) 654–667, https://doi.org/10.1080/15685551.2014.907621.
[56] J. Li, H. Sun, D. Sun, Y. Yao, F. Yao, K. Yao, Biomimetic multicomponent polysaccharide/nano-hydroxyapatite composites for bone tissue engineering, Carbohyd. Polym. 85 (2011) 885–894, https://doi.org/10.1016/j.carbpol.2011.04.015.
[57] H.M. Wang, C.T. Chou, Z.H. Wen, Z.R. Wang, C.H. Chen, M.L. Ho, Novel Biodegradable Porous Scaffold Applied to Skin Regeneration, PLoS ONE 8 (2013) 56330, https://doi.org/10.1371/journal.pone.0056330.
[58] A. Matica, G. Menghiu, V. Ostafe, Biodegradability of chitosan based products, New Front. Chem. 26 (2017) 75–86.
[59] S. Sprangers, V. Everts, Molecular pathways of cell-mediated degradation of fibrillar collagen, Matrix Biol. 75–76 (2019) 190–200, https://doi.org/10.1016/j.matbio.2017.11.008.
[60] F.H. Zulkifli, F.S. Jahir Hussain, M.S.B. Abdull Rasad, M.M. Yusoff, In vitro degradation study of novel HEC/PVA/collagen nanofibrous scaffold for skin tissue engineering applications, Polym. Degrad. Stab. 110 (2014) 473–481, https://doi.org/10.1016/j.polymdegradstab.2014.10.017.
[61] A. Sionkowska, M. Wisniewski, J. Skopinska, C.J. Kennedy, T.J. Wess, Molecular interactions in collagen and chitosan blends, Biomaterials 25 (2004) 795–801, https://doi.org/10.1016/S0142-9612(03)00595-7.
[62] A. Lončarević, M. Ivanković, A. Rogina, Lysozyme-Induced Degradation of Chitosan: The Characterisation of Degraded Chitosan Scaffolds, J. Tissue Eng. Regen. 1 (2017) 12–22, https://doi.org/10.14302/issn.2640-6403.jtrr-17-1840.
[63] L. Roseti, V. Parisi, M. Petretta, C. Cavallo, G. Desando, I. Bartolotti, B. Grigolo, Scaffolds for bone tissue engineering: State of the art and new perspectives, Mater. Sci. Eng. C 78 (2017) 1246–1262, https://doi.org/10.1016/j. msec.2017.05.017.
[64] V. Samouillan, A. Lamure, C. Lacabanne, Dielectric relaxations of collagen and elastin in the dehydrated state, Chem. Phys. 255 (2000) 259–271, https://doi.org/10.1016/S0301-0104(00)00080-X.
[65] L. Bozec, M. Odlyha, Thermal denaturation studies of collagen by microthermal analysis and atomic force microscopy, Biophys. J. 101 (2011) 228–236, https://doi.org/10.1016/j.bpj.2011.04.033.
[66] A. Ressler, J. Ródenas-Rochina, M. Ivanković, H. Ivanković, A. Rogina, G. Gallego Ferrer, Injectable chitosan-hydroxyapatite hydrogels promote the osteogenic differentiation of mesenchymal stem cells, Carbohydr. Polym. 197 (2018) 469–477, https://doi.org/10.1016/j.carbpol.2018.06.029.
[67] R. B. Attasgah, B. Velasco-Rodríguez, A. Pardo, J. Fernández-Vega, L. Arellano-Galindo, L. C. Rosales-Rivera, G. Prieto, S. Barbosa, J. F. A. Soltero, M. Mahmoudi, P. Taboada, Development of functional hybrid scaffolds for wound healing applications, iScience 25 (2022) 104019. Doi: https://doi.org/10.1016/j.isci.2022.104019.
[68] P. Bełdowski, M. Przybyłek, A. Sionkowska, P. Cysewski, M. Gadomska, K. Musiał, A. Gadomski, Effect of chitosan deacetylation on its affinity to type III collagen: a molecular dynamics study, Materials 15 (2022) 463, https://doi.org/10.3390/ma15020463.
[69] E.E. Golub, K., Boesze-Battaglia The role of alkaline phosphatase in mineralization, Curr. Opin. Orthop. 18 (2007) 444–448, https://doi.org/10.1097/BCO.0b013e3282630851.
[70] M.J. Seibel, Biochemical markers of bone turnover part I: Biochemistry and variability, Clin. Biochem. Rev. 26 (2005) 97–122.

[71] S. Vimalraj, Alkaline phosphatase: Structure, expression and its function in bone mineralization, Gene 754 (2020), 144855, https://doi.org/10.1016/j.gene.2020.144855.
[72] C.M. Murphy, G.H. Haugh, F.J. O'Brien, The effect of mean pore size on cell attachment, proliferation and migration in collagen-glycosaminoglycan scaffolds for bone tissue engineering, Biomaterials 31 (2010) 461–466, https://doi.org/10.1016/j.biomaterials.2009.09.063.
[73] C.M. Murphy, F.J. O'Brien, Understanding the effect of mean pore size on cell activity in collagen-glycosaminoglycan scaffolds, Cell Adh Migr. 4 (2010) 377–381, https://doi.org/10.4161/cam.4.3.11747.
[74] A.S. Mao, J.W. Shin, D.J. Mooney, Effects of substrate stiffness and cell-cell contact on mesenchymal stem cell differentiation, Biomaterials 98 (2016) 184–191, https://doi.org/10.1016/j.biomaterials.2016.05.004.
[75] A. Infante, C.I. Rodríguez, Osteogenesis and aging: lessons from mesenchymal stem cells, Stem Cell Res. Ther. 9 (2018) 244, https://doi.org/10.1186/s13287-018-0995-x.
[76] D. Qin, N. Wang, X.G. You, A.D. Zhang, X.G. Chen, Y. Liu, Collagen-based biocomposites inspired by bone hierarchical structures for advanced bone regeneration: ongoing research and perspectives, Biomater. Sci 10 (2022) 318–353, https://doi.org/10.1039/D1BM01294K.
[77] B. Kaczmarek, A. Sionkowska, Chitosan/collagen blends with inorganic and organic additive - A review, Polym. Adv. Technol. 37 (2018) 2367–2376, https://doi.org/10.1002/adv.21912.
[78] A. Karakeçili, S. Korpayev, K. Orhan, Optimizing Chitosan/Collagen Type I/Nanohydroxyapatite Cross-linked Porous Scaffolds for Bone Tissue Engineering, Appl. Biochem. Biotechnol. 194 (2022) 3843–3859, https://doi.org/10.1007/s12010-022-03962-0.